Available online at www.sciencedirect.com
ScienceDirect
Journal of Power Sources 161 (2006) 565–572
JOURNAL OF POWER SOURCES
www.elsevier.com/locate/jpowsour

Electrochemical intercalation of lithium into polypyrrole/silver vanadium oxide composite used for lithium primary batteries

Jong-Won Lee, Branko N. Popov *

Center for Electrochemical Engineering, Department of Chemical Engineering, University of South Carolina, Columbia, SC 29208, USA

Received 10 February 2006; received in revised form 21 March 2006; accepted 28 March 2006
Available online 8 May 2006

Abstract

Hybrid composites of polypyrrole (PPy) and silver vanadium oxide (SVO) used for lithium primary batteries were chemically synthesized by an oxidative polymerization of pyrrole monomer on the SVO surface in an acidic medium. The composite electrode exhibited higher discharge capacity and better rate capability as compared with the pristine SVO electrode. The improvement in electrochemical performance of the composite electrode was due to PPy which accommodates lithium ions and also enhances the SVO utilization. Chronoamperometric and ac-impedance measurements indicated that lithium intercalation proceeds under the mixed control by interfacial charge transfer and diffusion. The enhanced SVO utilization in the composite electrode results from a facilitated kinetics of interfacial charge transfer in the presence of PPy.

Keywords: Silver vanadium oxide; Polypyrrole; Lithium primary batteries

1. Introduction

Silver vanadium oxide (SVO), $Ag_2V_4O_{11}$, shows high gravimetric/volumetric energy densities [1,2]. When SVO is used as a positive electrode in Li/SVO batteries in implantable cardioverter-defibrillators, it performs most of the time at low power and occasionally delivers one or more high power pulses. SVO is capable of delivering about 50 J within 5–10 s and in case of a continuous current drain on the order of microamperes for at least five years [3]. It also provides an electrode potential curve with multiple plateaus, which allows accurately to predict the lifetime of the battery.

The synthesis methods of SVO are divided broadly into two categories – decomposition and combination reaction methods [4–7]. The former method uses decomposable silver compounds such as silver nitrate/nitrite, and hence it is inevitably accompanied by the evolution of toxic NO_x gas during the heat-treatment. In the combination reaction method, silver oxide Ag_2O reacts at about 520 °C with vanadium pentoxide V_2O_5 in 1:2 molar ratio without liberating any gaseous products. It has been reported [4,7] that a combination reaction leads to a well-crystallized SVO with higher surface area, when compared with the material synthesized using the decomposition reaction.

Seven moles of lithium can be theoretically inserted into SVO, yielding a discharge capacity of ca. 315 mAh g^{-1} [8]; however, much lower utilization of SVO is typically attained, especially at high discharge rates. The internal cell resistance drastically increases with progressing discharge, resulting in a poor power capability of the Li/SVO cells [2,3]. Attempts were made in the literature to improve the electrochemical performance of the SVO electrodes by optimizing the synthesis process [5,6] and by introduction of substitution atoms such as Na [9] or Sr [10].

It has been reported [11–20] that an improvement of the electrocatalytic properties of the active material is observed due to a synergetic effect of a conducting organic polymer and transition metal oxides. Our previous studies [19] indicated that polypyrrole (PPy)-doped cathodes for Li-ion batteries have improved performance when compared to that of the virgin material. It has been also shown [20] that PPy is electrochemically active in the potential range between 2.0 and 3.5 V versus Li^+/Li. Recent studies have demonstrated that pyrrole monomer can be oxidatively polymerized on the surfaces of $LiMn_2O_4$ [13,14], V_2O_5 [15] and $Co_{0.2}CrO_x$ [19] in acidic aqueous media with using

* Corresponding author. Tel.: +1 803 777 7314; fax: +1 803 777 8265.
E-mail address: popov@engr.sc.edu (B.N. Popov).

0378-7753/$ – see front matter © 2006 Elsevier B.V. All rights reserved.
doi:10.1016/j.jpowsour.2006.03.062

no oxidizing additives. Such PPy/oxide composites have been reported to markedly increase power capability and cyclability [13–15,19]. PPy/oxide composites were prepared by a chemical oxidation of pyrrole monomer in the oxide-dispersed aqueous solutions. Also, ferric chloride/perchlorate and ammonium peroxydisulfate have been used as oxidizing agents for chemical polymerization of pyrrole monomer [18,20,21].

In the present work a hybrid of PPy/SVO composite was synthesized in an attempt to increase the discharge capacity and improve rate capability of the SVO positive electrode. The PPy/SVO composite electrodes were prepared by an oxidative polymerization of pyrrole monomer on the SVO surface in an acidic medium. The composite electrodes which contain different PPy contents were subjected to extensive characterizations to evaluate their structures, compositions and electrochemical performance. Chronoamperometric and ac-impedance measurements were performed to understand the lithium intercalation in PPy/SVO composite electrode.

2. Experimental

2.1. Preparation of PPy/SVO composites

SVO was prepared by using a combination reaction of Ag_2O and V_2O_5. A mixture of Ag_2O (99 + %, Alfa Aesar) and V_2O_5 (99.995 %, Alfa Aesar) in 1:2 molar ratio was heat-treated in either N_2 or air at 520 °C for 24 h. As-heat-treated sample with a dark brown color was then pulverized by grinding into fine powders. The SVO powder specimens synthesized in N_2 and air are denoted as SVO(N) and SVO(A), respectively.

The composite specimens of PPy and SVO were chemically synthesized by an oxidative polymerization of pyrrole monomer on the SVO surface as follows: the SVO(A) powders prepared in an air atmosphere were dispersed in a 1 M $HClO_4$ solution, followed by bubbling with N_2 for 30 min. Then various concentrations of liquid pyrrole (98%, Aldrich) were slowly injected into the SVO(A)-containing solution during vigorous magnetic stirring. The resulting PPy/SVO(A) composite powders with a black color were collected by filtration, and they were thoroughly rinsed first with a 1 M $HClO_4$ solution and then with deionized water, followed by drying under vacuum at 80 °C for 12 h.

2.2. Materials characterizations

In order to identify the crystal structures of the synthesized powder specimens, X-ray diffraction (XRD) patterns were recorded with an automated Rigaku diffractometer using Cu K_α radiation over the scanning angle range of 10°–60° at the scan rate of 4° min^{-1}. Fourier transform-infrared (FT-IR) spectra were performed on pellets by using a Nicolet 4700 FT-IR spectrometer under transmittance mode. Thermogravimetric analysis (TGA) was conducted to determine the PPy content in composite using a Perkin-Elmer TGA7 thermogravimetric analyzer. The powder specimens were heated in a helium flow from room temperature to 500 °C at the scan rate of 5 °C min^{-1}.

2.3. Electrochemical experiments

The active material powders were mixed with 5 wt.% carbon black (acetylene, 99.9 %, Alfa Aesar) and 5 wt.% polytetrafluoroethylene (PTFE, Aldrich) to prepare a pellet with a diameter of 1 cm. A three-electrode electrochemical cell was employed for the electrochemical experiments. Both the reference and counter electrodes were constructed from lithium foil (electrochemical grade, FMC Corporation), and 1 M $LiPF_6$-DME/PC (50:50 vol.%, Ferro Corporation) was used as the electrolyte. The assembly of cells was performed in a glove box filled with purified argon gas.

Galvanostatic discharge experiments were carried out with an Arbin BT-2043 battery test station at various current densities with the cut-off potential being 1.5 V versus Li^+/Li. Chronoamperometric technique and electrochemical impedance spectroscopy (EIS) were performed using an EG&G PAR model 273 potentiostat combined with a Solartron 1255 frequency response analyzer. Chronoamperometric and impedance measurements were run by applying a potential drop of 25 mV and by applying an ac-amplitude of 5 mV peak-to-peak over the frequency range from 10 mHz to 100 kHz, respectively.

3. Results and discussion

3.1. Characterizations of PPy/SVO composite electrodes

Fig. 1 (a)–(c) presents powder XRD patterns of pristine SVO(N), SVO(A) and PPy/SVO(A) composite, respectively. The XRD patterns in Fig. 1 (a)–(c) are in good agreement with the pattern of the stoichiometric $Ag_2V_4O_{11}$ phase reported in literature [4,22]. When compared with the XRD pattern for SVO(A), the pattern for SVO(N) shows two additional peaks at about 22.6° and 25.1° both of which are attributed to the non-

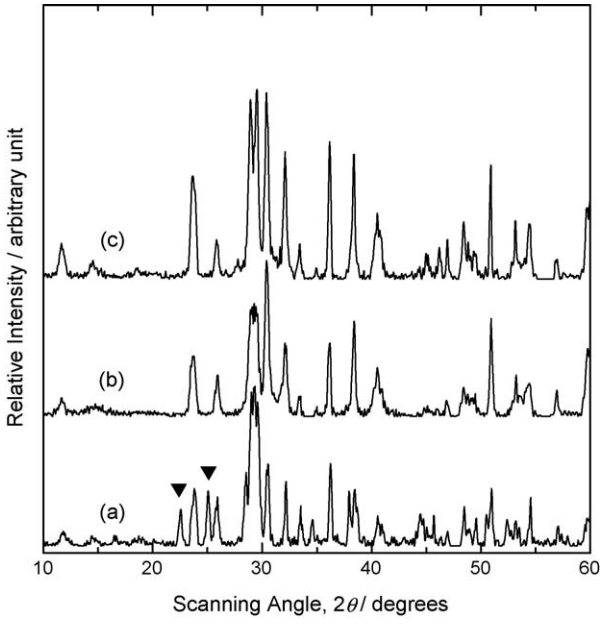

Fig. 1. XRD patterns of (a) SVO(N), (b) SVO(A) and (c) PPy/SVO(A) powder specimens. The arrows in (a) represent the peaks due to the $Ag_{1.2}V_3O_8$ phase.

stoichiometric $Ag_{1.2}V_3O_8$ phase. On the basis of a ternary phase diagram for Ag_2O–V_2O_5–V_2O_4, the appearance of $Ag_{1.2}V_3O_8$ phase in SVO(N) can be explained by a 'sprouting phenomenon' which refers to the phase transformation of $Ag_2V_4O_{11-y}$ to $Ag_{1.2}V_3O_8$ during heat-treatment in an inert atmosphere [23].

Since the extra electrons of the double bond in a conjugated system are free to move through the polymer chain, PPy is an inherent conducting polymer. However, in order to have a high electrical conductivity it should exist in the oxidized form [21]. In a deaerated $HClO_4$ solution containing pyrrole and SVO, oxidative polymerization of pyrrole monomer should take place on the SVO surface, leading to PPy-coated SVO composite. During polymerization, the following processes may occur to compensate the positive charges developed on the oxidized form of PPy: (i) a specific adsorption of ClO_4^- ions on the SVO surface and (ii) the formation of V^{4+} species on the SVO surface [11]. Accordingly, both the specifically adsorbed ClO_4^- ions and the negatively charged SVO act as dopants during the polymerization of pyrrole monomer. Since the XRD pattern of PPy/SVO(A) composite is exactly the same as that of pristine SVO(A), the results indicated that a small amount of V^{4+} species does not induce any significant structural modification of SVO(A) during the polymerization process.

Fig. 2 (a) and (b) show the FT-IR spectra obtained for the KBr-diluted pellets of pristine SVO(A) and PPy/SVO(A) composite, respectively. In both spectra, the characteristic absorption bands of the V–O–V and V=O vibrations are observed at approximately 750 and 925 cm^{-1}, respectively [24]. In addition, the FT-IR spectrum of PPy/SVO(A) composite exhibits two absorption bands around 1050 and 1190 cm^{-1} which can be assigned to the N–H and C–H in-plane vibrations in PPy, respectively [14].

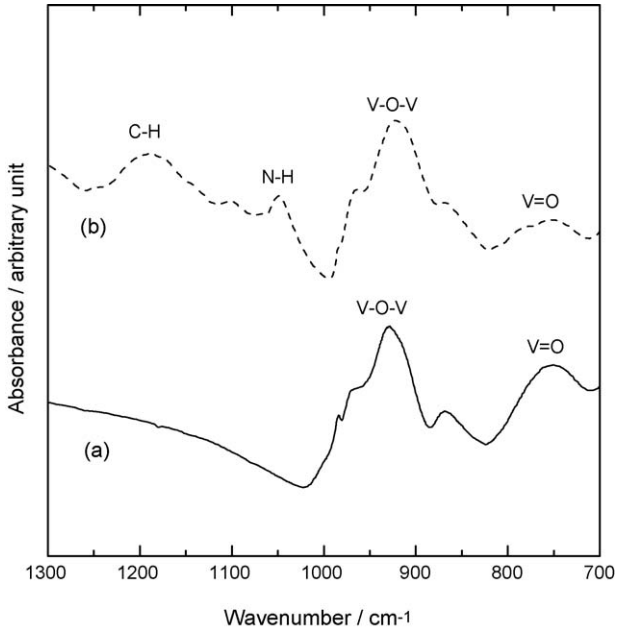

Fig. 2. FT-IR spectra measured on the KBr-diluted pellets of (a) SVO(A) and (b) PPy/SVO(A).

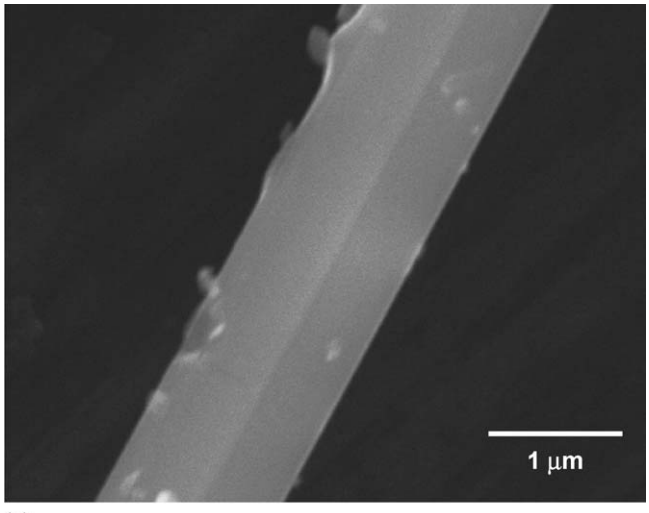

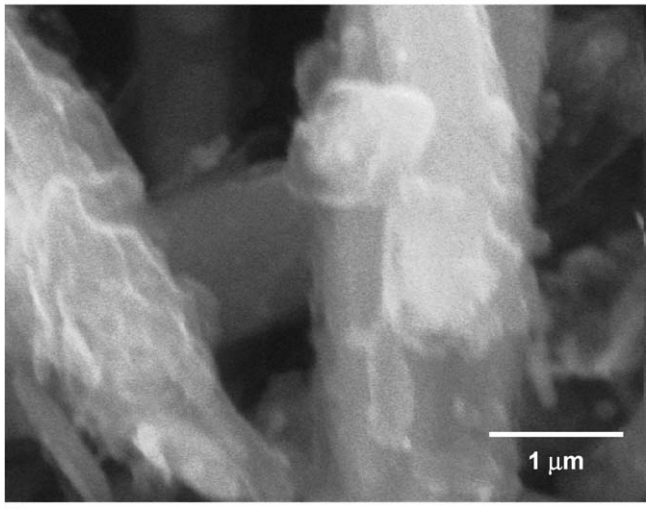

Fig. 3. SEM micrographs of (a) SVO(A) and (b) PPy/SVO(A).

This result confirms that SVO can be successfully used as an oxidizing agent to polymerize pyrrole monomer on its surface in an acidic $HClO_4$ solution, leading to the PPy/SVO composite electrode.

Fig. 3 (a) and (b) give SEM images of pristine SVO(A) and PPy/SVO(A) composite, respectively. The SEM micrograph of SVO(A) shows a needle-like crystallite with smooth surface. When compared with pristine SVO(A), PPy/SVO(A) composite exhibits rougher surface, indicating the presence of PPy on the SVO(A) surface.

The PPy content in the PPy/SVO(A) composite electrode was determined by estimating the weight loss of the composite material during a temperature scan carried out from room temperature to 500 °C in a helium flow. Fig. 4 (a) presents the sample weights as a function of temperature, measured for bare SVO(A), bare PPy and PPy/SVO(A) composite during TGA. As shown in Fig. 4(a), a bare PPy completely decomposes in the temperature range between 400 and 450 °C [19], whereas no weight loss is observed for bare SVO(A)

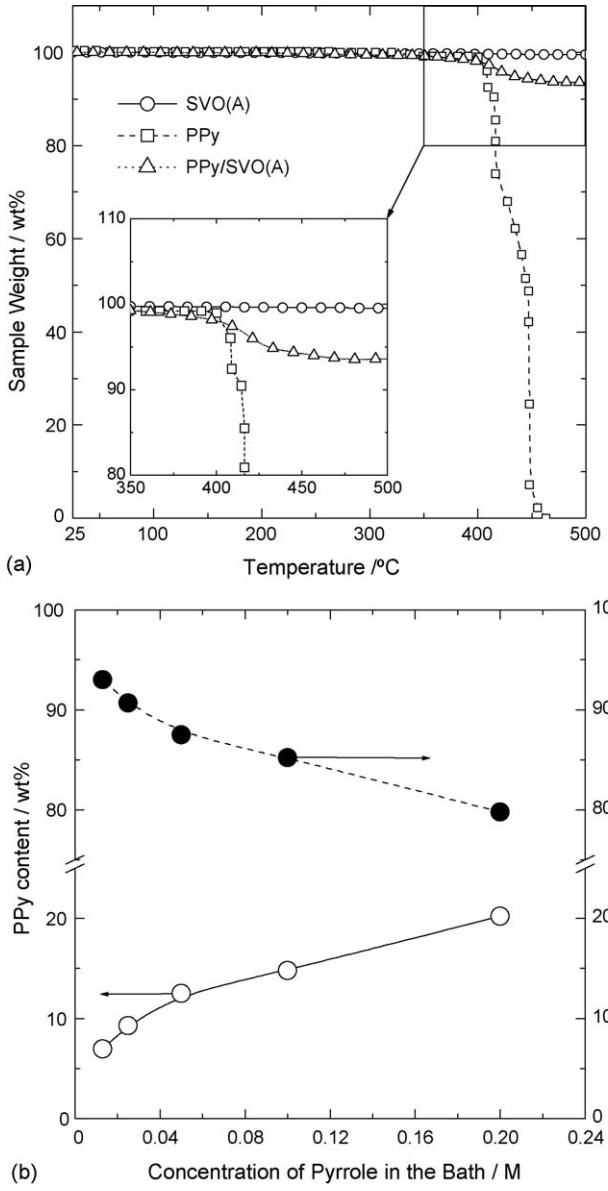

Fig. 4. (a) Weight losses of SVO(A), PPy and PPy/SVO(A) measured during TGA and (b) plots of the PPy and SVO(A) contents in the composite electrode against the liquid pyrrole concentration in the polymerization bath.

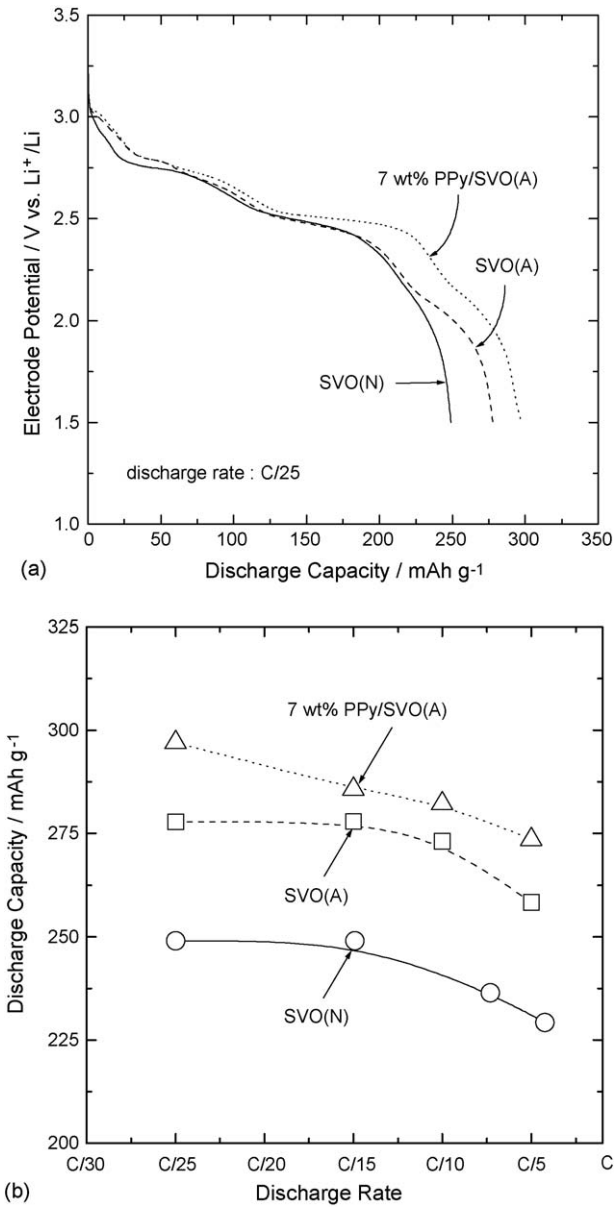

Fig. 5. (a) Galvanostatic discharge curves at the rate of C/25 and (b) specific discharge capacities as a function of the discharge rate, obtained for SVO(N), SVO(A) and 7 wt.% PPy/SVO(A). The specific discharge capacity was calculated based on only the weight of active material.

over the whole temperature range. For PPy/SVO(A) composite, a drastic weight loss occurs at approximately 420 °C due to the decomposition of PPy. Any complication arising from the presence of ClO_4^- ions is not seen in Fig. 4(a). The results indicated that TGA can be successfully used to determine the amount of PPy (wt.%) in the PPy/SVO(A) composite electrode.

Fig. 4 (b) shows the amounts of PPy and SVO(A) in the composite electrode as a function of the liquid pyrrole concentration injected into the polymerization bath. As the concentration of pyrrole monomer increases to 0.2 M, the PPy content gradually increases up to 20.2 wt.%. The composite electrodes with 0–15 wt.% PPy were subjected to extensive electrochemical characterization studies.

3.2. Electrochemical performances of PPy/SVO composite electrodes

Fig. 5(a) and (b) presents the galvanostatic discharge curves obtained at C/25 rate and the discharge capacity versus rate dependence, respectively. The discharge curves were recorded on three types of electrodes: pristine SVO(N), SVO(A) and 7 wt.% PPy/SVO(A) composite electrode. The value of the specific discharge capacity was calculated based on the weight of the active material rather than the weight of pellet with conductive carbon and organic binder.

The results presented in Fig. 5 (a) and (b) indicate that three distinct potential plateaus are observed at 2.8, 2.5 and 2.1 V versus Li^+/Li. The observed plateaus correspond to the reduction

reactions of (i) Ag^+ to Ag, (ii) V^{5+} to V^{4+} (and V^{4+} to V^{3+}) and (iii) V^{4+} to V^{3+}, respectively [25]. Besides the fact that PPy is electrochemically active in the potential range between 2.0 and 3.5 V versus Li^+/Li, the galvanostatic discharge curve of bare PPy shows that as the lithium content (or discharge capacity) increases, the potential decreases monotonously without showing any distinct potential plateau regions [20].

The discharge capacity determined at the cut-off potential of 1.5 V versus Li^+/Li increases in the order of pristine SVO(N), SVO(A) and PPy/SVO(A) composite. Since only four moles of lithium can be electrochemically intercalated into $Ag_{1.2}V_3O_8$ [26], a lower discharge capacity of the pristine SVO(N) electrode we believe is attributable to the presence of $Ag_{1.2}V_3O_8$ phase which is confirmed by the XRD pattern in Fig. 1 (a). The PPy/SVO(A) composite electrode shows the highest discharge capacity of ca. 297 mAh g^{-1}. As shown in Fig. 5(a), the second potential plateau of PPy/SVO(A) composite is larger when compared to that of pristine SVO(A), which indicates that PPy contributes mainly to an increase in the discharge capacity of the composite electrode at approximately 2.5 V versus Li^+/Li. It is also of importance to note that the improvement in the discharge capacity of PPy/SVO(A) composite as shown in Fig. 5 (b) remains over a wide range of discharge rates, indicating an enhanced rate capability of the composite material.

Fig. 6 (a) presents the discharge capacities of the PPy/SVO(A) composite electrodes which contain various PPy contents. For comparison, the theoretical dependence of the discharge capacity on the PPy content is also presented in Fig. 6(a). Besides the fact that bare PPy is known to be electrochemically active for lithium intercalation, it typically has much lower capacity of ca. 72 mAh g^{-1} than the bare SVO [20], and hence the theoretical discharge capacity of PPy/SVO(A) composite should decrease linearly with increasing the PPy content. However, the galvanostatic discharge data in Fig. 6(a) clearly show that the discharge capacity of PPy reaches a maximum for PPy content between 7.0 and 12.5 wt.%.

The composite electrode yields higher discharge capacity than the pristine SVO(A) electrode. In case of PPy/SVO(A) composite, the synergic electrochemical performance exceeds the sum of PPy and SVO(A)'s individual performances indicating that besides the fact that PPy is electrochemically active (it possesses it's own capacity to intercalate lithium ions), it also promotes lithium insertion into SVO(A).

Fig. 6 (b) shows the utilization of SVO(A) in the composite electrode as a function of the PPy content. The utilization was calculated from the measured discharge capacity of PPy/SVO(A) by assuming a full utilization of PPy with a capacity of 72 mAh g^{-1}. The PPy content in the composite in the range of 7.0–12.5 wt.% causes SVO(A) to be fully utilized during the discharge process.

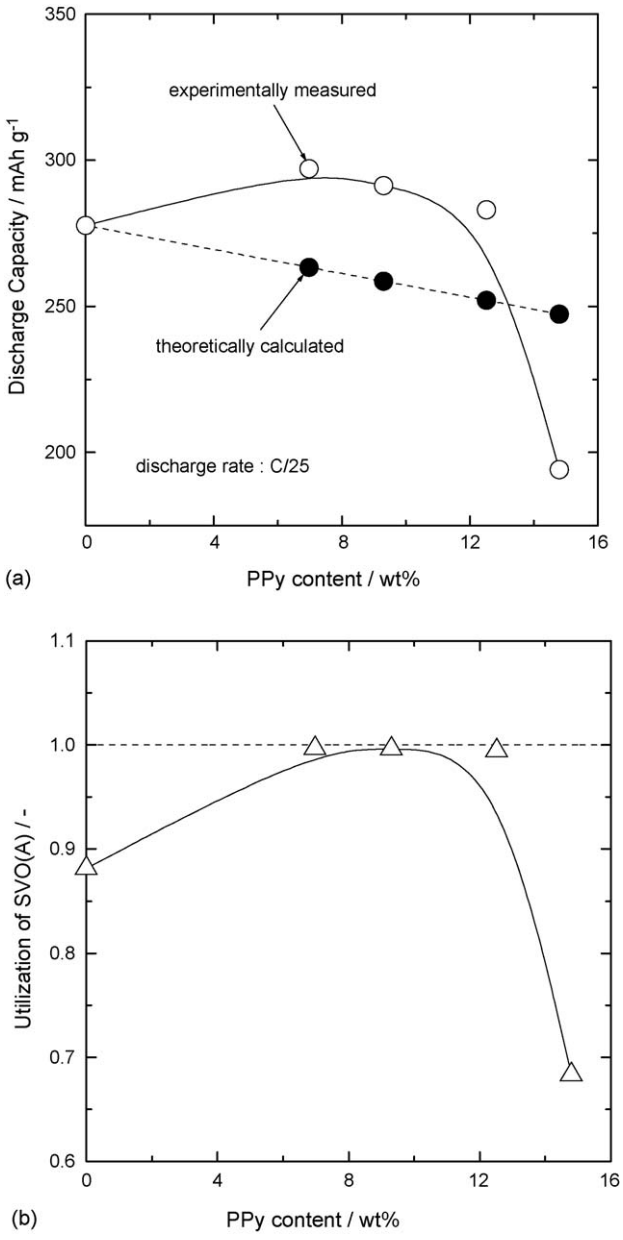

Fig. 6. (a) Theoretical and experimental discharge capacities of PPy/SVO(A) and (b) utilization of SVO(A) in PPy/SVO(A) as a function of the PPy content. The full utilization of PPy was assumed with a capacity of 72 mAh g^{-1}.

3.3. Kinetic studies on lithium intercalation into PPy/SVO composite electrodes

Chronoamperometry (potentiostatic current transient technique) was used to estimate the rate-determining steps which control the lithium intercalation. If lithium intercalation is controlled by diffusion within the bulk of the electrode, the relationship between the current I and time t is given by Cottrell equation [27]:

$$I(t) = \frac{Q\sqrt{\tilde{D}_{\mathrm{Li}}}}{L\sqrt{\pi}} t^{-1/2} \quad \text{for} \quad t \ll \frac{L^2}{\tilde{D}_{\mathrm{Li}}} \tag{1}$$

where Q is the total charge transferred over the whole lithium intercalation, $\tilde{D}_{\mathrm{Li}}$ is the chemical diffusivity of lithium while L denotes the diffusion length. According to Eq. (1), the Cottrell region is characterized by a plateau in the $It^{1/2}$ versus $\log t$ plot (Cottrell plot). Therefore, the Cottrell plot can provide a diagnostic tool for identifying the intercalation behavior of lithium.

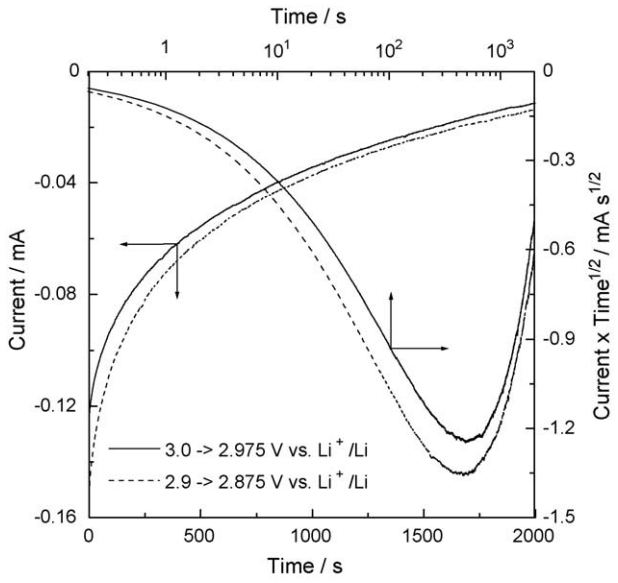

Fig. 7. Typical current responses of 7 wt.% PPy/SVO(A) to different potential steps.

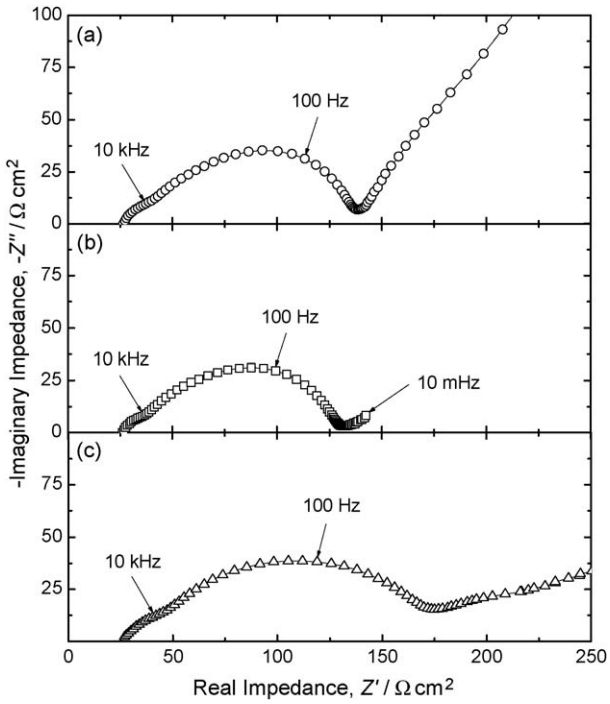

Fig. 8. Nyquist plots of the ac-impedance spectrum for 7 wt.% PPy/SVO(A) at different electrode potentials: (a) 3.4 V vs. Li$^+$/Li, (b) 2.8 V vs. Li$^+$/Li and (c) 2.0 V vs. Li$^+$/Li.

Fig. 7 presents typical chronoamperometric curves obtained for 7 wt.% PPy/SVO(A) composite electrode. The experiments were performed by shifting the applied potential from 3.0 to 2.975 V versus Li$^+$/Li and from 2.9 to 2.875 V versus Li$^+$/Li. The corresponding Cottrell plots were constructed from the chronoamperometric curves. Since any plateau region is absent throughout the entire intercalation time, one can conclude a non-diffusion-controlled process of lithium intercalation. Recently, this chronoamperometric behavior of intercalation compounds has been extensively discussed by Montella [28] and Lee and Pyun [29]. They have proposed that the Cottrell relation Eq. (1) is not valid in case when interfacial charge transfer and diffusion become simultaneously involved in the rate-determining steps of intercalation. Consequently, the non-Cottrell behavior in Fig. 7 suggests that lithium intercalation into the PPy/SVO(A) composite electrode is not controlled by diffusion alone, but rather it proceeds under the mixed control by the interfacial charge transfer and diffusion reactions.

In view of the mixed control process, the useful information that helps to understand the enhanced SVO(A) utilization in the composite electrode can be acquired by analyzing two kinetic parameters, namely the charge transfer resistance and the lithium diffusivity.

Fig. 8(a)–(c) demonstrates typical Nyquist plots of the ac-impedance spectrum obtained for 7 wt.% PPy/SVO(A) composite electrode. The electrode was potentiostatically polarized at 3.4, 2.8 and 2.0 V versus Li$^+$/Li, respectively, until a low steady-state current was attained. Next, the ac-impedance spectroscopy was performed at each of the polarizing potentials. Each of the ac-impedance spectra consists of two separated arcs in the high frequency range and a straight line inclined at constant angle to the real axis in the low frequency range. The magnitude of the first arc is almost independent of the electrode potential, while the second arc shows a strong potential-dependence. Various models have been proposed to explain such a two-arc behavior of the ac-impedance in intercalation compounds. It is generally accepted [25,30] that the first arc is mainly caused by the formation of the passive film on the surface of the oxide particle, and the second arc is ascribed to the interfacial charge transfer reaction.

A straight line at low frequencies is associated with semi-infinite diffusion of lithium in the electrode (Warburg impedance). The ideal diffusion impedance should exhibit the phase angle of 45°; however, according to Fig. 8, the absolute value of the phase angle for the measured diffusion impedance is higher than 45° at 3.4 V versus Li$^+$/Li, and it decreases to values lower than 45° with decreasing electrode potential. The decreasing tendency of the absolute phase angle with lowering electrode potential has also been observed for V_2O_5 [31]. The anomalous behaviors of diffusion impedance with absolute phase angles greater and lower than 45° can be explained in terms of the particle size (diffusion length) distribution [32,33] and of the activation energy distribution for diffusion through the electrode [31], respectively. The abnormal behaviors of diffusion impedance lie beyond the scope of this work.

Fig. 9 compares the plots of the charge transfer resistance for pristine SVO(A) and for 7 wt.% PPy/SVO(A) composite as a function of the electrode potential. The data were obtained by using complex nonlinear least squares (CNLS) fitting of the ac-impedance spectra. The charge transfer resistance of PPy/SVO(A) composite decreases drastically when compared to the pristine SVO(A) over the whole potential range. It is conceivable that an enhanced charge transfer kinetics results from a conductive PPy network on the SVO(A) surface.

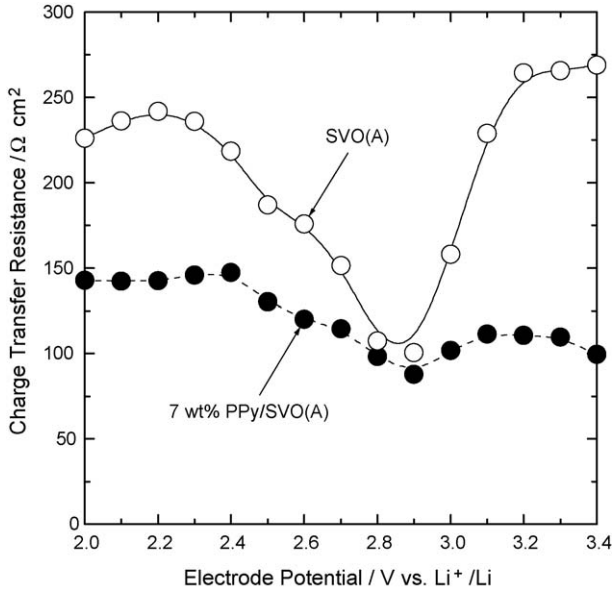

Fig. 9. Plots of the charge transfer resistance against the electrode potential, obtained for SVO(A) and 7 wt.% PPy/SVO(A).

Since the measured diffusion impedance deviates from the ideal Warburg behavior, it is not possible exactly to determine the chemical diffusivity of lithium $\tilde{D}_{Li}$ from the ac-impedance spectra. The value of $\tilde{D}_{Li}$ was alternatively evaluated from the potential transient and coulometric titration curve [34]:

$$\tilde{D}_{Li} = \frac{4}{\pi}\left(\frac{I_{app}V_M}{FA_g}\right)\left[\frac{(dE/dx)}{(dE/d\sqrt{t})}\right] \quad \text{for} \quad t \ll \frac{L^2}{\tilde{D}_{Li}} \tag{2}$$

where I_{app} is the applied current, V_M the molar volume of the electrode, F the Faraday constant, A_g the superficial geometric area of the electrode, E the electrode potential and x means the lithium content in the electrode.

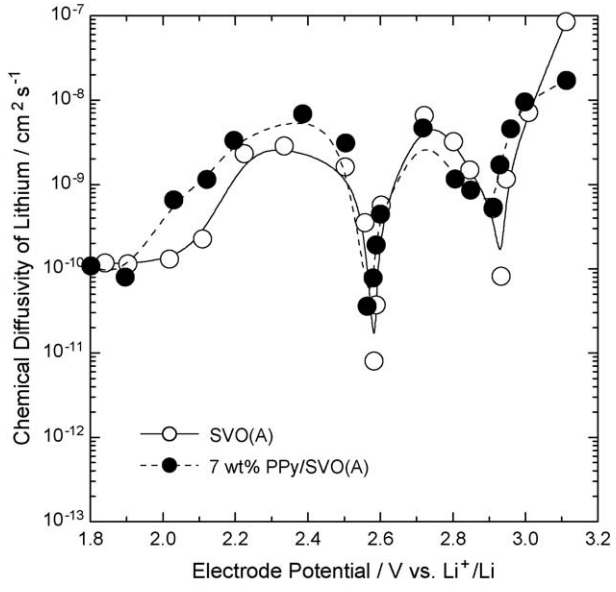

Fig. 10. Plots of the chemical diffusivity of lithium in SVO(A) and 7 wt.% PPy/SVO(A) with respect to the electrode potential.

The values of $\tilde{D}_{Li}$ for pristine SVO(A) and for 7 wt.% PPy/SVO(A) composite were plotted in Fig. 10 as a function of the electrode potential. The plots presented in Fig. 10 indicate that $\tilde{D}_{Li}$ for both tested materials has similar dependence on the applied electrode potential showing two minima at about 2.6 and 2.9 V versus Li^+/Li.

The results indicate that PPy facilitates the interfacial charge transfer kinetics by forming an effective conductive network on the SVO(A) surface and improves the utilization of the composite electrode. No significant influence of PPy on the diffusion kinetics of lithium was observed in this study.

4. Conclusions

PPy/SVO composite materials were chemically prepared by using SVO as an oxidizing agent to polymerize pyrrole monomer in an acidic $HClO_4$ solution. Galvanostatic discharge experiments showed that the composite electrodes with 7.0–12.5 wt.% PPy yield higher discharge capacity and rate capability when compared to the pristine SVO electrode. The utilization studies indicate that PPy facilitates the interfacial charge transfer and improves the utilization of the composite electrode. Chronoamperometric measurements proposed that lithium intercalation is simultaneously controlled by the interfacial charge transfer and diffusion reactions. The analyses of the ac-impedance spectra and the potential transients indicate that the charge transfer resistance is reduced by addition of PPy, while the lithium diffusivity remains nearly constant, regardless of the presence and absence of PPy. Thus, no significant influence of PPy on the diffusion kinetics of lithium was observed in this study.

Acknowledgements

Financial support provided by St. Jude Medical Co. is acknowledged gratefully. The FT-IR measurements were done by Yu Su at the Department of Chemical Engineering at the University of South Carolina.

References

[1] K.J. Takeuchi, A.C. Marschilok, S.M. Davis, R.A. Leising, E.S. Takeuchi, Coordin. Chem. Rev. 219–221 (2001) 283–310.
[2] A.M. Crespi, S.K. Somdahl, C.L. Schmidt, P.M. Skarstad, J. Power Sources 96 (2001) 33–38.
[3] A. Crespi, C. Schmidt, J. Norton, K. Chen, P. Skarstad, J. Electrochem. Soc. 148 (2001) A30–A37.
[4] A.M. Crespi, US Patent 5,221,453 (1993).
[5] R.A. Leising, E.S. Takeuchi, Chem. Mater. 5 (1993) 738–742.
[6] R.A. Leising, E.S. Takeuchi, Chem. Mater. 6 (1994) 489–495.
[7] A.M. Crespi, K. Chen, US Patent 6,130,005 (2000).
[8] E.S. Takeuchi, W.C. Thiebolt, J. Electrochem. Soc. 135 (1988) 2691–2694.
[9] J. Kawakita, K. Makino, Y. Katayama, T. Miura, T. Kishi, J. Power Sources 75 (1998) 244–250.
[10] J. Kawakita, R. Shimizu, Y. Katayama, T. Miura, T. Kishi, Solid State Ionics 123 (1999) 181–188.
[11] A.H. Gemeay, H. Nishiyama, S. Kuwabata, H. Yoneyama, J. Electrochem. Soc. 142 (1995) 4190–4195.
[12] S. Kuwabata, T. Idzu, C.R. Martin, H. Yoneyama, J. Electrochem. Soc. 145 (1998) 2707–2710.

[13] S. Kuwabata, S. Masui, H. Yoneyama, Electrochim. Acta 44 (1999) 4593–4600.
[14] A. Du Pasquier, F. Orsini, A.S. Gozdz, J.-M. Tarascon, J. Power Sources 81–82 (1999) 607–611.
[15] S. Kuwabata, S. Masui, H. Tomiyori, H. Yoneyama, Electrochim. Acta 46 (2000) 91–97.
[16] P. Gomez-Romero, Adv. Mater. 13 (2001) 163–174.
[17] P.R. Somani, R. Marimuthu, A.B. Mandale, Polymer 42 (2001) 2991–3001.
[18] C.-W. Kwon, A. Poquet, S. Mornet, G. Campet, J. Portier, J.-H. Choy, Electrochem. Commun. 4 (2002) 197–200.
[19] R.P. Ramasamy, B. Veeraraghavan, B. Haran, B.N. Popov, J. Power Sources 124 (2003) 197–203.
[20] G.X. Wang, L. Yang, Y. Chen, J.Z. Wang, S. Bewlay, H.K. Liu, Electrochim. Acta 50 (2005) 4649–4654.
[21] M. Omastová, M. Trchová, J. Kovářová, J. Stejskal, Synth. Met. 138 (2003) 447–455.
[22] K. West, A.M. Crespi, J. Power Sources 54 (1995) 334–337.
[23] P. Rozier, J. Galy, J. Solid State Chem. 134 (1997) 294–301.
[24] J.M. Lee, H.-S. Hwang, W.-I. Cho, B.-W. Cho, K.Y. Kim, J. Power Sources 136 (2004) 122–131.
[25] R.P. Ramasamy, C. Feger, T. Strange, B.N. Popov, J. Appl. Electrochem. 36 (2006) 487–497.
[26] J. Kawakita, Y. Katayama, T. Miura, T. Kishi, Solid State Ionics 99 (1997) 71–78.
[27] C.J. Wen, B.A. Boukamp, R.A. Huggins, W. Weppner, J. Electrochem. Soc. 126 (1979) 2258–2266.
[28] C. Montella, J. Electroanal. Chem. 518 (2002) 61–83.
[29] J.-W. Lee, S.-I. Pyun, Electrochim. Acta 50 (2005) 1777–1805.
[30] D. Aurbach, K. Gamolsky, B. Markovsky, G. Salitra, Y. Gofer, U. Heider, R. Oesten, M. Schmidt, J. Electrochem. Soc. 147 (2000) 1322–1331.
[31] K.-N. Jung, S.-I. Pyun, J.-W. Lee, Electrochim. Acta 49 (2004) 4371–4378.
[32] J.-W. Lee, S.-I. Pyun, Z. Metallkd. 96 (2005) 117–123.
[33] J.-P. Diard, B. Le Gorrec, C. Montella, J. Electroanal. Chem. 499 (2001) 67–77.
[34] W. Weppner, R.A. Huggins, J. Electrochem. Soc. 124 (1977) 1569–1578.